Modulation and Time-History-Dependent Adaptation Improves the Pick-and-Place Control of a Bioinspired Soft Grasper

Yanjun Li[1(✉)], Ravesh Sukhnandan[5], Hillel J. Chiel[2,3,4], Victoria A. Webster-Wood[5,6,7], and Roger D. Quinn[1]

[1] Department of Mechanical Engineering, Case Western Reserve University, Cleveland, OH, USA
yxl2259@case.edu
[2] Department of Biology, Case Western Reserve University, Cleveland, OH, USA
[3] Department of Neurosciences, Case Western Reserve University, Cleveland, OH, USA
[4] Department of Biomedical Engineering, Case Western Reserve University, Cleveland, OH, USA
[5] Department of Mechanical Engineering, Carnegie Mellon University, Pittsburgh, PA, USA
[6] Department of Biomedical Engineering, Carnegie Mellon University, Pittsburgh, PA, USA
[7] McGowan Institute for Regenerative Medicine, Carnegie Mellon University, Pittsburgh, PA, USA

Abstract. It is widely believed that adaptive peripheral neural control circuits and compliant peripheral biomechanics in biological systems are critical for their control of interactions with the environment. Inspired by the sea slug *Aplysia californica*'s adaptive feeding mechanism, we previously designed a pneumatically actuated soft grasper controlled by Synthetic Nervous Systems for pick and place manipulation. To guarantee the grasping success rate, the controller sends a fixed grasper radius command during grasper closure. However, such a strategy may generate overly high contact force for manipulating soft and fragile objects. To address this problem, we adopted velocity control circuitry to cap the contact force within a force threshold. Furthermore, inspired by the local modulation of *Aplysia* networks and muscles, we incorporated time-history-dependent control into the grasper controller. Such modulatory mechanisms allow the force threshold to adapt according to the external load. We evaluated the adaptive controller's performance in simulation and physical hardware. By comparing it with two baselines, we show the grasper can achieve high success rates for pick-and-place tasks and prevent high contact force when manipulating light objects in a simulation environment. Hardware experiments were also performed to demonstrate that the control network could be transferred to the real-world platform. These results sup-

This work was supported in part by the National Science Foundation (NSF) grant nos. FRR-2138873 and FRR-2138923 and by a GEM fellowship.

Y. Li and R. Sukhnandan—These authors contributed equally to the work.

N. S. Szczecinski et al. (Eds.): Living Machines 2024, LNAI 14930, pp. 351–367, 2025.
https://doi.org/10.1007/978-3-031-72597-5_24

port our hypothesis that soft, morphologically intelligent grasping robots with onboard bioinspired adaptation will improve grasping performance.

Keywords: Soft Robotics · Robotic Manipulation · Synthetic Nervous Systems · *Aplysia* · Neuromodulation.

1 Introduction

Controlling robots to manipulate complex and fragile objects remains an ongoing challenge in robotics. Humans and animals can complete a wide range of manipulation tasks with their soft peripheries. Due to the lack of such compliance, few robots with rigid end effectors and joints can achieve human-level safety and dexterity in manipulation [14,16,34]. Many contact-rich tasks, such as harvesting soft, fragile, and irregularly shaped fruits, still rely on humans [15]. Guided by the structure of biological systems, materials with soft properties have appeared with increasing frequency in the design of robots [1,8,26]. The compliance allows robots to conform to the objects they interact with, leading to stable contact and evenly distributed contact forces [3]. For example, soft graspers inspired by octopus tentacles and elephants have been developed [2,9]. However, these continuum robots are characterized by many degrees of freedom, making the state estimation and control computationally complex [4,31].

Inspired by the adaptive control of soft, many-degree-of-freedom peripheries in the sea slug *Aplysia californica* [17,32], we previously developed a soft grasper for pick-and-place tasks [27]. The grasper abstractly embodies the morphology and neural control of *Aplysia*'s feeding apparatus. With two layers of cylindrical McKibben actuators, it can conform to and envelop a grasped object. In addition, it can actively tune the contact stiffness by regulating air pressure in the internal cavity of soft jaws. We designed a neural network controller for the grasper and expressed the neural dynamics in the framework of Synthetic Nervous Systems (SNSs), a neural network model previously adopted in modeling the *Aplysia* feeding control circuits [21]. In this prior work, based on position and force sensory feedback, the controller can determine which subtask to complete and generate motor commands to move, open, or close the soft grasper. Force feedback is used to determine whether the object has been grasped or released but not actually leveraged to control the grasping behavior in real time. For robust grasping, the network sends a fixed, pre-determined grasper radius command. This strategy, however, often leads to overly high contact force for picking up lightweight and soft objects. Moreover, it cannot adaptively increase the force applied to pick up heavier objects. In contrast, animals like *Aplysia* can adaptively modify the properties of muscles and joints in response to environmental loading and feedback through neuromodulation [22]. Capturing key features of neuromodulation, such as slow but long-lasting activation enhancement due to repetitive firing of presynaptic neurons, may help to ensure a safer interaction between the grasper and the environment.

In this work, we integrated modulation mechanisms into the SNS controller to implement time-history-dependent contact force adaptation. We modified the

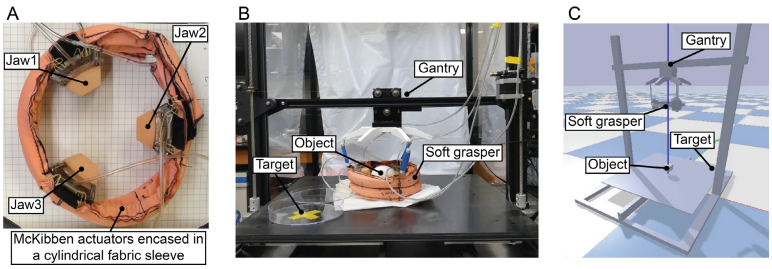

Fig. 1. The hardware and simulation platform for testing the bioinspired soft grasper. (A) Top view of the grasper. (B) The gantry system for pick-and-place manipulation. (C) The simulation model of the system (built in the Pybullet engine).

synaptic connection so that the soft grasper generated a fixed closing speed for grasping and stopped squeezing once the contact force reached a force threshold. This modification allows the grasper to maintain contact force around the force threshold. In addition, we incorporated modulatory synapses to mediate the output of sensory neurons. The modulatory mechanism allows the grasper to temporarily increase the force threshold for the next attempt if the current grasping attempt fails. Our simulation and experimental results suggest that the controller presented here can adaptively regulate the contact force according to the load. Meanwhile, the grasper can achieve higher success rates for grasping objects with various weights when adaptability is enabled. Due to the dynamic range of force capabilities, the integration of the bio-inspired soft grasper and control algorithms can be a plausible candidate for manipulating fragile, slippery, or complex objects, such as harvesting and processing agricultural products.

2 Methods

Bioinspired Soft Grasper and Simulation Environment. The *Aplysia*-inspired soft grasper and simulation environment were previously described in [27]. Briefly, the grasper abstracted the principles of circumferential contraction of *Aplysia*'s jaw lumen and the ability to sense and tune contact forces found in *Aplysia*'s grasper. Circumferential contraction was achieved through the use of McKibben actuators encased in a cylindrical fabric sleeve (Fig. 1**A**). Three soft jaws, made of Smooth-On Vytaflex 30A whose stiffness could be independently tuned were fixed to the inside of the sheath to provide sensing and tuning of contact forces. When the jaws deformed due to contact, the corresponding increase in pressure was measured by pressure sensors. The soft grasper was connected to a Cartesian gantry robot (Fig. 1**B**) to move the grasper for pick-and-place tasks [20].

To facilitate training of the Synthetic Nervous System (SNS) controller, we developed a model of the grasper robot in PyBullet (Fig. 1**C**). To simulate the radial motion of the jaws with the contraction of the circumferential McKibben actuators, the jaws were placed on linear motor-powered prismatic joints. The soft jaws were represented as rigid bodies with a pressure-dependent contact

stiffness [27]. The training of the SNS controller was implemented based on Neural Circuit Policies toolbox for PyTorch [19].

Synthetic Nervous Systems We built the controller for the soft grasper based on Synthetic Nervous Systems (Fig. 2A), a type of neural network model inspired by neurons' biophysical mechanisms for encoding information and conducting computation [30]. In SNSs, signals are typically represented by variables with biophysical meaning, such as membrane potential or neuronal firing rates. Various conductance-based mechanisms can then be incorporated to perform operations on these variables [21,23,29]. Below is a discretized version of equations governing the dynamics of an SNS network with n neurons[1] [27]:

$$\boldsymbol{y}_t = \phi(\boldsymbol{h}_t) \tag{1}$$

$$\hat{\boldsymbol{\tau}}_t = \frac{\boldsymbol{\tau}}{1 + \boldsymbol{V}\boldsymbol{y}_{t-1}} \tag{2}$$

$$\boldsymbol{z}_t = \frac{\Delta}{\hat{\boldsymbol{\tau}}_t + \Delta} \tag{3}$$

$$\hat{\boldsymbol{h}}_t = \frac{\boldsymbol{b} + \boldsymbol{W}\boldsymbol{y}_{t-1}}{1 + \boldsymbol{V}\boldsymbol{y}_{t-1}} \tag{4}$$

$$\boldsymbol{h}_t = (1 - \boldsymbol{z}_t) \odot \boldsymbol{h}_{t-1} + \boldsymbol{z}_t \odot \hat{\boldsymbol{h}}_t \tag{5}$$

where Δ is the time step, t is the sample time. $\boldsymbol{h}_t = \left[U_1, \cdots, U_n\right]^\top$ denotes membrane potential of neurons. ϕ in Eq. (1) denotes the activation function[2] relating membrane potential $\boldsymbol{h}_t$ to neurons' normalized firing rates $\boldsymbol{y}_t$. The time constants $\boldsymbol{\tau} = \left[\tau_1, \cdots, \tau_n\right]^\top$ and the bias term $\boldsymbol{b} = \left[b_1, \cdots, b_n\right]^\top$ are parameters determining the intrinsic neuronal dynamics, while the other two parameters, the matrix $\boldsymbol{V}$ denoting the input strength of synaptic conductance and the matrix $\boldsymbol{W}$ denoting the product of reversal potential and input strength of synaptic conductance, determine the synaptic dynamics of SNS neurons. Eqs. (2)–(4) describe the relationship between the output variable $\boldsymbol{y}_t$ and three intermediate variables $\hat{\boldsymbol{\tau}}_t$, $\boldsymbol{z}_t$, and $\hat{\boldsymbol{h}}_t$, which are called the effective time constant vector, update vector, and candidate activation vector in the field of artificial neural networks [13].

Due to their advantages in biological plausibility and computational capability, SNSs have been applied in building neurocircuitry models of animals [5,21,24] and controlling robots [7,10,12,20,27,28]. Designing an SNS controller requires finding appropriate parameter values for $\boldsymbol{\tau}$, $\boldsymbol{b}$, $\boldsymbol{W}$, and $\boldsymbol{V}$. Both analytical methods [29,30] and supervised learning methods [20] have been reported to construct SNSs with desired dynamics for robotic control. In particular, Eqs. (1)–(5) can be viewed as an extension of traditional artificial neural network (ANN) models such as multilayer perceptrons (MLPs) and continuous-time recurrent neural networks [6], meaning that SNSs can be trained as other ANN models using gradient descent methods.

[1] In Eqs. (1)–(5), addition, subtraction, and division are performed element-wise. $\odot$ denotes element-wise product, a binary operation that multiplies elements corresponding to the same rows and columns of given matrices.

[2] We selected HardTanh activation function $\phi(\boldsymbol{h}_t) = \min(1, \max(0, \boldsymbol{h}_t)$ (min() and max() are the element-wise minimum and maximum, respectively).

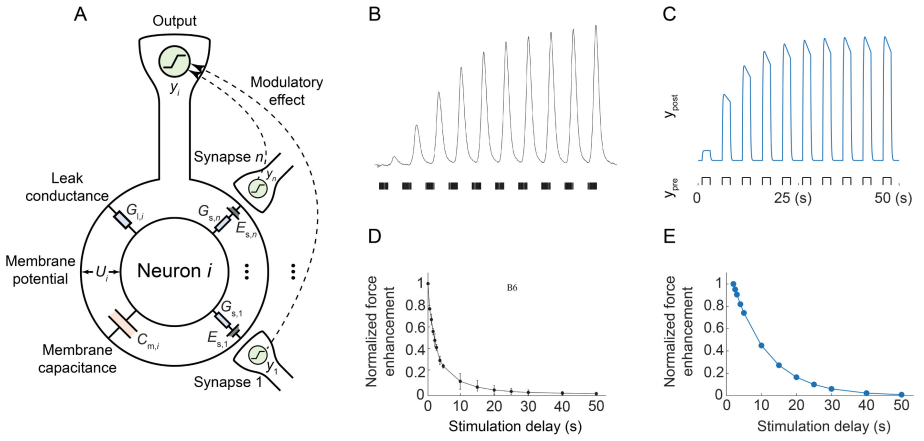

Fig. 2. Synthetic Nervous Systems and the time-history-dependent control mechanism. (A) Schematic of the ith neuron in the SNS network. The membrane capacitance ($C_{\mathrm{m},i}$) and leak conductance ($G_{\mathrm{l},i}$) define the time constant of the neuron. $E_{\mathrm{s},ij}$ and $G_{\mathrm{s},ij}$ denote the reversal potential and input strength of the jth synaptic conductance, respectively. Dashed lines indicate the potential modulatory effects of presynaptic neurons. (B) Repeated firing of B6 enhances the *Aplysia* I3 muscle forces generated by the same neuron during swallowing-like patterns (Fig. 8 in [22] by Hui Lu et al., reproduced under CC BY 4.0). (C) With the time-history-dependent control mechanism, repeated firing of the presynaptic SNS neuron enhances the activity of the postsynaptic SNS neuron generated by the same neuron. (D) Force enhancement decays as the interpattern interval increases in *Aplysia* I3 muscle (Fig. 11 in [22] by Hui Lu et al., reproduced under CC BY 4.0). (E) Activation enhancement decays as the inter-pattern interval increases in SNSs. For (C) and (E), modulation parameters are set to $\tau_{\mathrm{m}} = 1$ s, $t_d = 2$ s, $\beta = 0.1$, $k = 40$, and $\alpha = 1$.

Time History Dependent Control. In this work, we introduced time-history-dependent control into SNSs by augmenting the governing equations. It has been previously demonstrated that time-history-dependent changes in the periphery and neural activity can prepare animal muscles for subsequent actions [22]. For example, repetition of neural activation to the I3 muscle of the sea slug *Aplysia* in biting-like patterns, which would otherwise generate little force, can prepare the muscle to generate higher force during subsequent swallowing-like patterns (Fig. 2B). Incorporating such mechanisms inspired by local modulation into the grasper controller allows the robot to generate robust and adaptive pick-and-place behavior even in the absence of higher-level control. To modulate SNS outputs, we scaled the original activation given by Eq. (1) using the following transformation

$$\boldsymbol{y}_t = (1 + \boldsymbol{k} \odot \boldsymbol{a}_t)^{\boldsymbol{\alpha}} \odot \phi(\boldsymbol{h}_t) \tag{6}$$

where $\boldsymbol{k}$ is the modulation strength for each neuron. The exponent $\boldsymbol{\alpha} \in \{1, -1\}$ determines whether the modulation amplifies ($\boldsymbol{\alpha} = 1$) or represses $\boldsymbol{\alpha} = -1$ the output. The dynamics of the normalized modulation activity $\boldsymbol{a}_t$ in our model can be expressed as

$$\boldsymbol{u}_t = \widetilde{\boldsymbol{W}} \boldsymbol{y}_{t-t_\mathrm{d}} \tag{7}$$

$$\widetilde{\boldsymbol{u}}_t = \frac{\boldsymbol{u}_t}{\boldsymbol{\beta} + (1 - \boldsymbol{\beta}) \odot \boldsymbol{u}_t}, \; 0 \leq \boldsymbol{\beta} \leq 1 \tag{8}$$

$$\widetilde{\boldsymbol{\tau}}_t = \frac{\widetilde{\boldsymbol{u}}_t}{\boldsymbol{u}_t} \odot \boldsymbol{\tau}_\mathrm{m} \tag{9}$$

$$\widetilde{\boldsymbol{z}}_t = \frac{\Delta}{\widetilde{\boldsymbol{\tau}}_t + \Delta} \tag{10}$$

$$\boldsymbol{a}_t = (1 - \widetilde{\boldsymbol{z}}_t) \odot \boldsymbol{a}_t + \widetilde{\boldsymbol{z}}_t \odot \widetilde{\boldsymbol{u}}_t \tag{11}$$

Equations (7)–(10) are a discretized version of the pure time delay process $\boldsymbol{u}(t) = \boldsymbol{y}(t - \boldsymbol{t}_\mathrm{d}\Delta)$ and first-order differential equations $\frac{\mathrm{d}\boldsymbol{a}}{\mathrm{d}t} + \frac{1}{\boldsymbol{\tau}_\mathrm{m}} [\boldsymbol{\beta} + (1 - \boldsymbol{\beta})\boldsymbol{u}(t)] \, \boldsymbol{a}(t) = \frac{1}{\boldsymbol{\tau}_\mathrm{m}} \boldsymbol{u}(t)$ [33], where $\widetilde{\boldsymbol{W}}$ is the mask matrix that determines which presynaptic neuron has modulatory effects. Due to the indirect connection between receptors and effectors, the onset of neuromodulatory effects in animals is generally slow [18]. The discrete-time delay, $\boldsymbol{t}_\mathrm{d}$, was incorporated here to capture this phenomenon. Another characteristic of neuromodulation is its long-lasting effects. The time course of decay can last many seconds or even minutes (Fig. 2D, [22]). In our model, $\boldsymbol{\beta}$ is the parameter we can use to adjust the rate of decay. Since $0 \leq \boldsymbol{\beta} \leq 1$, the rate constant associated with this first-order dynamics ($\frac{1}{\widetilde{\boldsymbol{\tau}}_t}$) linearly increases with increased excitation $\boldsymbol{u}(t)$. Therefore, the time course of decay is slower than the time course of buildup, and the parameter $\boldsymbol{\beta}$ controls the ratio of the time constant for buildup in the full modulation case (i.e., $\boldsymbol{u}(t) = 1$, $\widetilde{\boldsymbol{\tau}} = \boldsymbol{\tau}_\mathrm{m}$) and the time-constant for decay in the full relaxation case (i.e., $\boldsymbol{u}(t) = 0$, $\widetilde{\boldsymbol{\tau}} = \frac{\boldsymbol{\tau}_\mathrm{m}}{\boldsymbol{\beta}}$). Figure 2C and 2E demonstrate the activation enhancement and enhancement decay, respectively, of a postsynaptic neuron that is excited by a presynaptic neuron and modulated by the same neuron using the modulation-inspired mechanism. The results suggest the model can qualitatively capture the modulation behavior of muscle forces observed in *Aplysia*.

Control for Pick-and-Place Tasks. Integrating SNSs and time-history-depen-dent control, we designed a soft grasper controller for a basic pick-and-place task (Fig. 3). The task requires the grasper to pick up an object at a prespecified position and then place it in a target position. The pick-and-place controller was taken from our previous work [27], with modifications for the grasper radius commands control and an extension for force threshold modulation. Inspired by neural circuits for *Aplysia* feeding control, the control network has a hierarchical structure and sparse synaptic connections. Neurons in the sensory layer calculate the distance between the grasper, object, and target. Some are also responsible for detecting if contact force is above predefined thresholds. Based on this information, the command neuron layer determines which subtask,

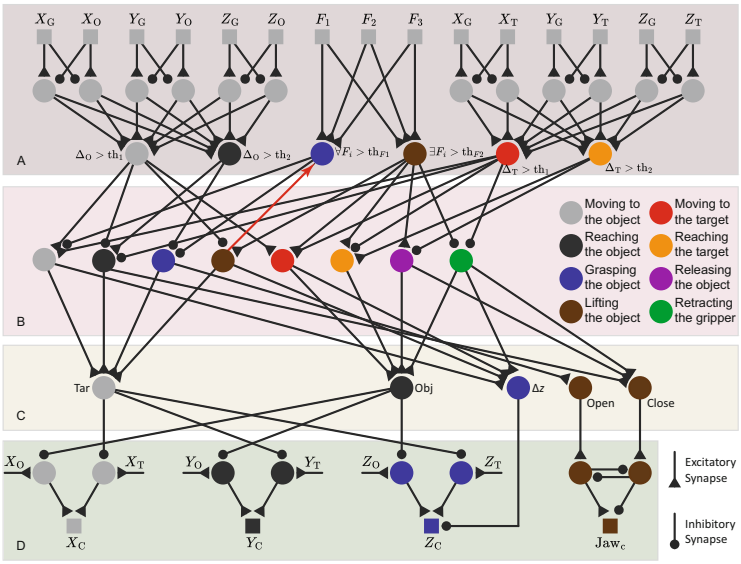

Fig. 3. The SNS controller for the pick-and-place task. (A) Sensory neuron layer. (B) Command neuron layer. (C) Interneuron layer. (D) Motor neuron layer. The sensory layer passes the object position (X_O, Y_O, Z_O), the target position (X_T, Y_T, Z_T), the grasper position (X_G, Y_G, Z_G), and the contact force of three soft jaws (F_1, F_2, F_3) to the network controller. Nodes labeled with the same symbol represent the same sensory neuron. The modulatory synapse is highlighted in red. (Color figure online)

or phase, the grasper should fulfill. Each command neuron in this layer selectively activates neurons in the following interneuron layer, which in turn activates or inhibits motor neurons in the motor neuron layer to implement corresponding motor primitives. Activities of motor neurons encode normalized commands for the grasper position and grasper radius.

We used velocity control to produce the joint radius command for its superiority in contact force regulation. Our previous controller sends a fixed grasper radius command for grasping and moving the object for robust grasp. However, such a strategy would not allow it to adaptively increase the force applied to a heavy object. Moreover, the fixed grasper radius may lead to excessively high contact force when interacting with fragile and soft objects, making them break or deform without returning to their original shape. To address this challenge, the controller presented in this paper adopts velocity control to mediate the opening and closing of the grasper instead of directly generating grasper radius commands. We modified the synaptic connections so that the controller specifies a negative jaw velocity (increasing the grasper closure) when grasping the object and a positive jaw velocity when releasing the object (decreasing the grasper closure). To allow regrasps after potential failures, the controller also specifies a positive jaw velocity in the reaching-the-object phase. For other phases, the velocity commands remain zero. Jaw velocity commands are finally sent to an

integration subnetwork [30] to obtain the grasper radius command. With velocity control, the grasper will stop increasing the grasper closure after the contact force achieves the force threshold. This mechanism enables the contact force to stay close to a predefined value, preventing the grasper from squeezing fragile objects with too much force.

We also leveraged the time-history-dependent control to increase the grasping performance in different scenarios. Using the above velocity control can cap the value of contact force to a predefined force threshold, but grasping objects with different weights, coefficient of friction, and attachment conditions may require different force thresholds. For example, the force threshold appropriate to pick up a soft and light object is generally too low for a heavy object. We added modulatory synapses from the lifting-the-object command neuron to force sensory neurons to overcome the limitation. Such local modulation can decrease the gain of force sensory neurons ($\boldsymbol{\alpha} = -1$ in Eq.(6)) and equivalently increase the force threshold when reaching the object. Furthermore, the effect of modulation can accumulate in the short term due to the slow decay, meaning the force threshold will become higher and higher until the grasper implements a successful grasp. With time-history-dependent control, the soft grasper has the ability to adjust the contact force level for various objects.

Validation of Modulation Controller. We first conducted a simulation to demonstrate the effectiveness of the adaptable pick-and-place controller. The task required the soft grasper to pick up a cubic object weighing 500 g from its initial position to a target position in the Pybullet engine. To further evaluate the SNS controller, we tested its performance in simulation scenarios with different ratios of heavy objects and compared its success rate and contact force with two baselines. In the Pybullet environment, we generated 11 groups of objects with the ratio of heavy objects (P_h) varying from 0% to 100%. Each group contains 20 cubic objects, among which $20P_\mathrm{h}$ are heavy, and $20(1 - P_\mathrm{h})$ are light. We randomly selected the mass of a heavy object from 500 g to 1000 g and the mass of a light object from 50 g to 300 g. For performance comparison, we consider the following baselines: 1) the SNS controller using the position control for the grasper radius command. This baseline reported in [27] sends a fixed grasper radius command for jaw closure, 2) the SNS controller using the velocity control for the grasper radius command. This baseline is identical to the controller presented in this work, except it does not have modulatory synapses to implement time-history-dependent control. We evaluated how the two baselines and the adaptive SNS controller with time-history-dependent control mechanisms performed on the 11 groups of objects three times. We defined a pick-and-place task as successful if the object was moved to the target position within 15 s. It is possible that the system may get stuck in some phases of the pick-and-place task. Therefore, we set a cut-off time for the manipulation to meet to be considered as successful. In the Pybullet simulation, this time (15 s) allows the grasper to complete the pick-and-place task with at most five attempts to grasp the object. For each simulation, we recorded the maximal contact force generated

by the soft grasper and then normalized it with the highest contact force in all experiments. Table 1 lists the main parameters of SNS controllers in simulation.

We also designed hardware experiments to test the effect of modulation on increasing the applied force on subsequent grasps. It should be noted that there was a sim-to-real gap due to the difficulties in modeling the soft contact between the object and the grasper. The heaviest objects the physical soft grasper robot could manipulate were generally lighter than those in the Pybullet simulation. Thus, we performed pick-and-place trials on a 173.4 g object, which was lighter than the object (500 g) we used in the simulation. The modulation gain of the SNS, $\boldsymbol{k}$, was set to one of two conditions. The first condition, $\boldsymbol{k} = 0$, causes no modulation of the sensory feedback and hence no increase in force on subsequent grasp attempts. The second condition, $\boldsymbol{k} = 29$, results in modulation of the sensory feedback, and hence we expect an increase in grasping force on subsequent grasp attempts. We performed 10 pick-and-place trials for each case. The target object was a 3D printed rectangular prism (cross-section 35 mm $\times$ 35 mm, weight 173.4 g). Controls and data were sampled at a rate of 16.7 Hz. The time-history-dependent SNS controller was used with the following parameters. The time constant of the grasper, τ_{grasp}, was set to 5 s. The sensory gain of the SNS, K_{SNS}, was set to 10. The raw pressure values at the jaws were thresholded to prevent false triggering from noise, where the thresholds, $\boldsymbol{P_{th}} \in \mathbf{R}^3$, are $[0.010, 0.020, 0.029]$ psi. The raw pressure readings were scaled by a constant, $K_p = 1750$. Hence, the contact force fed back to the SNS, $\boldsymbol{F_C}$, is given by the following equation:

$$\boldsymbol{F_C} = max(K_p \cdot (\boldsymbol{P_C} - \boldsymbol{P_{th}}), 0) \tag{12}$$

where $\boldsymbol{P_C} \in \mathbf{R}^3$ is the contact pressures at the jaws, and $max()$ is the element-wise maximum. We determined the values of $\boldsymbol{k} = 29$, $K_{SNS} = 10$, $\tau_{grasp} = 5$ s and $K_p = 1750$ via manual tuning to obtain the desired behavior.

3 Results

Simulation Results. With modulatory mechanisms, the soft grasper controlled by the SNS network can successfully move the 500 g object to the target position (Fig. 4). At t = 4 s, the grasper reached the object position and started its first attempt to grasp. However, the object slipped out of the grasper at t = 5 s due to low force thresholds encoded in the sensory neuron layer. Detecting the loss of contact, the SNS controller switched from the lifting-the-object phase to the reaching phase and performed a regrasp at t = 5.5 s. Synapses from the lifting-the-object command neuron also modulated neurons in the sensory neuron, allowing the encoded force thresholds to increase temporarily. This led to a successful grasp on the second attempt. The soft grasper then lifted the object up and completed the pick-and-place manipulation.

Baseline comparisons suggest that the SNS controller with modulation can adaptively regulate the contact force for objects with different masses (Fig. 5).

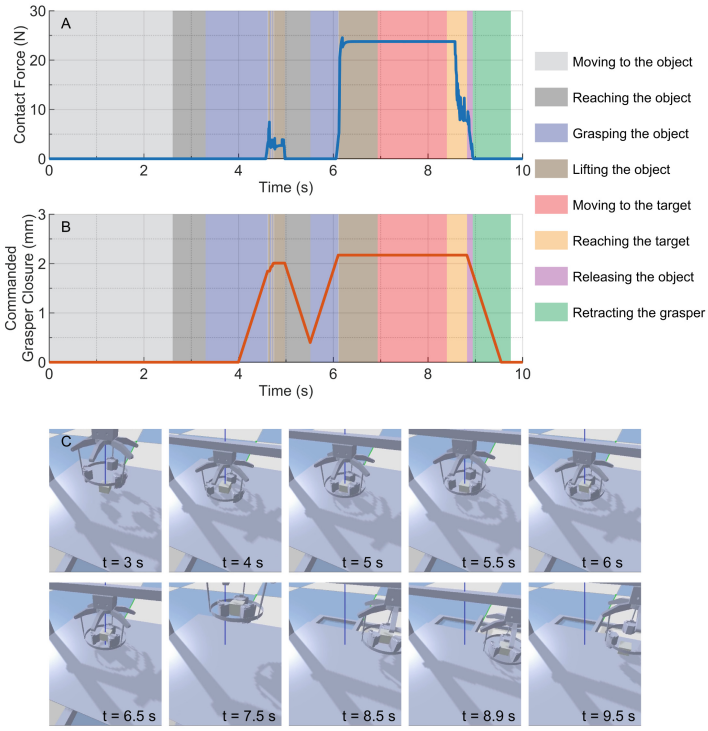

Fig. 4. The soft grasper controlled by the SNS network for pick-and-place manipulation in simulation. The object to pick up was a 500 g cube. Two attempts to grasp the object can be identified according to the contact force curve (A), the commanded grasper closure curve (B), and snapshots of the robot (C). The first attempt to grasp the object (t = 5 s) failed due to the low contact force. The grasper then attempted another grasp (t = 6 s). With the modulatory effect and increased force threshold, the grasper could successfully lift the object and move it to the target position. The colors of shades indicate the phases of the manipulation.

The baseline using position control for jaw closure always sends the highest grasper radius change for grasper closure. This strategy guarantees a high success rate for all groups of objects but may also lead to unnecessary high or even hazardous contact force for manipulating light and delicate objects. On the other hand, the baseline using velocity control for jaw closure can cap the contact force once it approaches a fixed threshold. This mechanism keeps contact forces at a low level for all groups of objects and achieves a high success rate for groups with few heavy objects. However, this baseline achieves a low success rate for groups with a high proportion of heavy objects due to the fixed force threshold. The integration of velocity control and time-history-dependent control alleviates the problem by local modulation. If the current threshold is insufficient to pick up the object, the SNS controller will try to regrasp it and use the

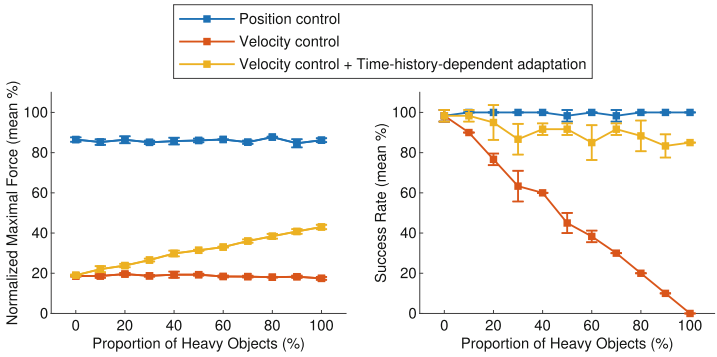

Fig. 5. Performance of the baseline and adaptive control methods for different proportions of heavy objects. Error bars represent standard error of the mean (SEM). Note that velocity control combined with time-history-dependent control results in both a high success rate (right panel) and a lower maximum normalized force (left panel).

modulatory mechanism to increase the threshold. This process repeats until the soft grasper implements a successful grasp. Therefore, as the proportion of heavy objects increases, the adaptive SNS controller can generate higher contact force to maintain a high success rate.

Experimental Results. The SNS with modulation of the force thresholds ($\boldsymbol{k} = 29$) was able to successfully pick up the object 6 out of the 10 trials (Table 1). In contrast, the SNS without modulation ($\boldsymbol{k} = 0$) failed on all 10 attempts. The transition pressure and commanded grasper closure on the 1st attempt for $\boldsymbol{k} = 29$ and $\boldsymbol{k} = 0$ were similar (Fig. 6). At the final attempt, successful grasps with modulation showed a large increase in the commanded grasper closure and, consequently, an increase in the jaw pressure, which can be taken as a proxy for the contact force imparted by the grasped object on the soft grasper (Fig. 6). Without modulation, however, on the final attempt, both the commanded grasper closure and the maximum change in pressure remained close to the values in the initial attempt (Fig. 6), which was insufficient for a successful pick-up.

The increase in success with modulation of the force thresholds (Table 1, Fig. 6) aligns with the simulation results (Fig. 5). However, because of differences in the mechanics of the simulation and the actual soft body mechanics of the real grasper, neither the contact force or grasper closure command behaviors exactly replicate the simulation. These differences also required substantial hand-tuning of the parameters of the SNS controller to obtain the desired behavior of failing on the 1st attempt and getting a successful grasp to complete the pick-and-place motion on subsequent attempts. Future work will further improve the simulation platform to better capture these mechanics and minimize the sim-to-real gap. Furthermore, control schemes like iterative learning control (ILC) that

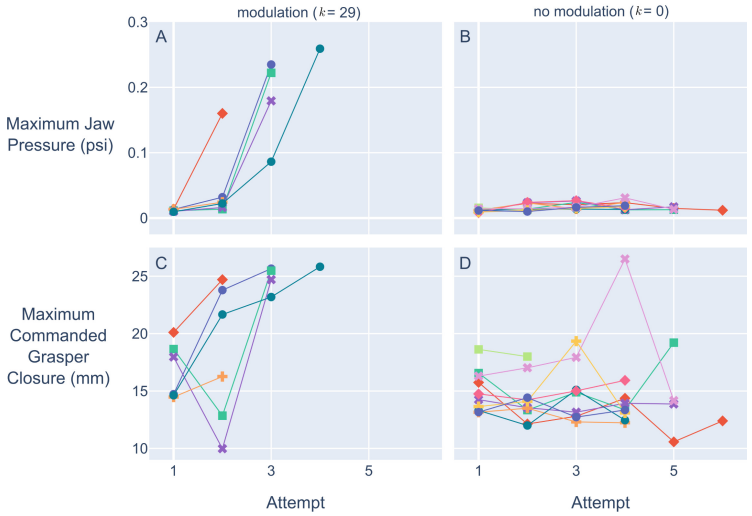

Fig. 6. Maximum jaw pressure experienced by the grasper (top row) and maximum commanded grasper closure (bottom row) for $\boldsymbol{k} = 29$ and $\boldsymbol{k} = 0$ during the lifting-the-object phase. A larger grasper closure indicated that the grasper contracted radially and consequently squeezed the object more. 6 of 10 trials for $\boldsymbol{k} = 29$ were successful (left column). All 10 trials for $\boldsymbol{k} = 0$ were unsuccessful (right column). Successful grasps with $\boldsymbol{k} = 29$ showed increased jaw pressure on subsequent grasp attempts after initial failure on attempt 1 (A). Without modulation, the contact pressure remained consistently small (B). Likewise, when $\boldsymbol{k} = 29$, the final commanded grasp closure for successful grasps was greater than the commanded closure on the initial attempt (C). No such trend was observed when there was no modulation (D). Different color-symbol combinations represent different trials. A comparison of a typical successful and unsuccessful trial with modulation is shown in Fig. 7.(Color figure online)

use rollouts on hardware to optimize control inputs may be used to fine-tune the gains in a more automated way [11,25].

Though more successful than the case without modulation, grasping failures were still observed. These failures were primarily caused by the inability of the grasper to properly trigger a transition from the lifting-the-object to the reaching-the-object phase because the grasper did not deflate enough during the descent of the re-attempt, and so the jaws made contact with the object (Fig. 7). The grasper would then begin to inflate while stuck on top of the object and would not register a large enough change in contact pressure to trigger the transition from the grasping-the-object phase to the lifting-the-object phase (Fig. 7). This can be remedied in the future by augmenting the soft jaws with other contact sensors distributed spatially around the grasper to detect contact events that are not only localized at the jaws, which are most sensitive to radially directed contact forces. This additional sensory information could help the grasper to reason about such unexpected contact events.

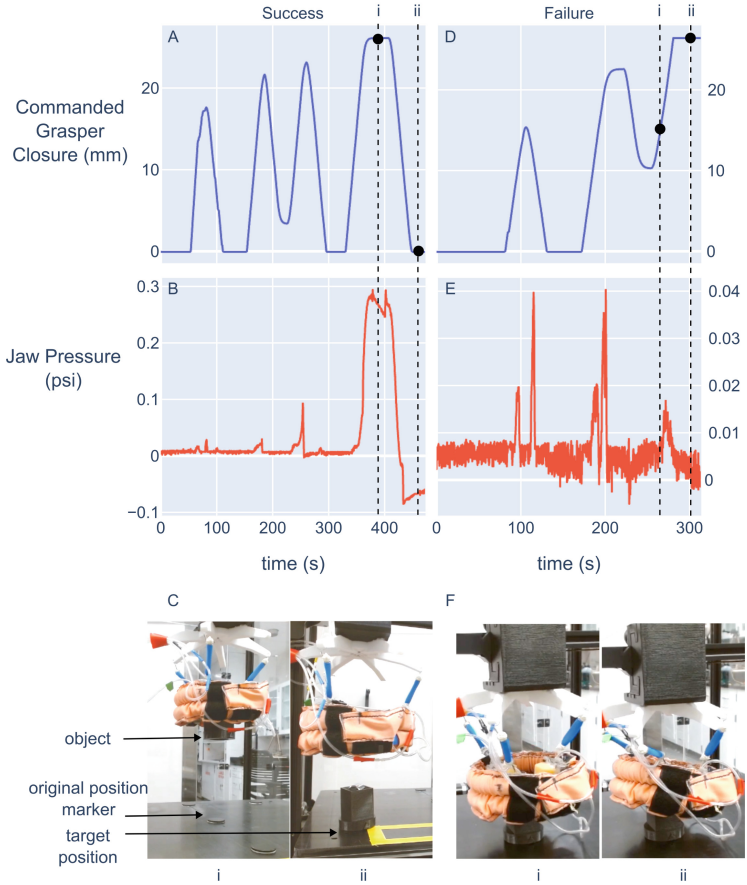

Fig. 7. Comparison of commanded grasper closure and jaw pressure for a successful (left column) and unsuccessful (right column) pick-and-place trial with the SNS modulation of force thresholds ($\boldsymbol{k} = 29$). While the commanded grasper closure shows an increase with subsequent attempts for both successful and unsuccessful grasp (A and D), the jaw pressure at the final attempt is much different (note the different y-axis scales of B and E). In the successful case, the grasper was able to deflate and successfully grasp the object (C, i) and deposit it at the target position (C, ii). In the failure case, the grasper did not fully deflate during the reaching-the-object phase of the reattempt, which caused the jaws to get stuck on top of the object (F, i). The commanded closure increased, but since the object was below the jaws, insufficient contact forces were generated to transition to the lifting-the-object phase (F, ii).

Table 1. Summary of SNS parameters and success rate for pick-and-place experiments in simulation and real-world. Modulation gain $\boldsymbol{k} = 0$ means the modulation mechanism is turned off. τ_{grasp} controls the gain of the integration subnetwork, thus determining the jaw closure velocity. K_{SNS} controls the initial force threshold.

	$\boldsymbol{k}$	τ_{grasp} (s)	K_{SNS}	K_p	Success Rate (%)
*Simulation	4	3.3	10	–	90.5, $n = 660$
	0	3.3	10	–	48.3, $n = 660$
*Real-world	29	5	10	1750	60, $n = 10$
	0	5	10	1750	0, $n = 10$

4 Conclusions and Future Work

In this work, we incorporated bioinspired modulation mechanisms into the framework of Synthetic Nervous Systems and applied them to the pick-and-place control of a soft grasper. The adaptable SNS controller also used velocity control for jaw closure so that it could exploit the contact force information to regulate the pressure between the grasper and the object. The combination of velocity control and time-history-dependent-control endowed the controller with the capability to adaptively change the force threshold, which is critical for safe interaction with a wide range of objects. Simulation results in the Pybullet environment demonstrated the adaptable SNS controller can achieve high success rates for the pick-and-place tasks while avoiding excessively high contact force. We also successfully transferred the controller to the physical grasper and demonstrated the benefits of using time-history-dependent control.

To reduce the sim-to-real gap, we will focus on improving the fidelity of the simulation to the physical robot. The temporal dynamics of the closure muscles and the soft jaws can be included in the simulation environment in future work. Future work will also explore the tunable stiffness of the soft grasper and the plasticity of the SNS. Due to the usage of soft deformable jaws, our grasper can generate tunable stiffness decoupled from the positional state of the closure muscle. This feature could be critical for safe robot-environment interaction and has drawn much attention in the research of agriculture robots, prostheses, and exoskeletons. In this work, we set the pressure applied to the internal cavity of the jaw to a pre-defined value. Therefore, the advantage of tunable stiffness was not leveraged. Our future work will explore the benefit of real-time stiffness tuning in manipulation tasks. In addition to the local modulation, we aim to integrate short-term and long-term plasticity into SNS networks so that the controller can implement online learning. The plasticity rules will allow the controller to learn appropriate parameters (such as the grasper closing speed and the modulatory gain) from interaction with objects and use its experience of success and failure to improve the control policy over time.

References

1. Bolívar-Nieto, E.A., Thomas, G.C., Rouse, E., Gregg, R.D.: Convex optimization for spring design in series elastic actuators: From theory to practice. In: 2021 IEEE/RSJ International Conference on Intelligent Robots and Systems (IROS), pp. 9327–9332 (2021). https://doi.org/10.1109/IROS51168.2021.9636427
2. Cianchetti, M., Calisti, M., Margheri, L., Kuba, M., Laschi, C.: Bioinspired locomotion and grasping in water: the soft eight-arm octopus robot. Bioinspiration Biomimetics **10**(3), 035003 (2015). https://doi.org/10.1088/1748-3190/10/3/035003
3. Ciocarlie, M., Miller, A., Allen, P.: Grasp analysis using deformable fingers. In: 2005 IEEE/RSJ International Conference on Intelligent Robots and Systems, pp. 4122–4128 (2005). https://doi.org/10.1109/IROS.2005.1545525
4. Della Santina, C., Duriez, C., Rus, D.: Model-based control of soft robots: a survey of the state of the art and open challenges. IEEE Control Syst. Mag. **43**(3), 30–65 (2023). https://doi.org/10.1109/MCS.2023.3253419
5. Deng, K., Szczecinski, N.S., Arnold, D., Andrada, E., Fischer, M.S., Quinn, R.D., Hunt, A.J.: Neuromechanical model of rat hindlimb walking with two-layer cpgs. Biomimetics **4**(1), (2019). https://doi.org/10.3390/biomimetics4010021
6. Funahashi, K., Nakamura, Y.: Approximation of dynamical systems by continuous time recurrent neural networks. Neural Netw. **6**(6), 801–806 (1993). https://doi.org/10.1016/S0893-6080(05)80125-X
7. Goldsmith, C.A., Szczecinski, N.S., Quinn, R.D.: Neurodynamic modeling of the fruit fly drosophila melanogaster. Bioinspiration Biomimetics **15**(6), 065003 (2020). https://doi.org/10.1088/1748-3190/ab9e52
8. Goncalves, A., Kuppuswamy, N., Beaulieu, A., Uttamchandani, A., Tsui, K.M., Alspach, A.: Punyo-1: Soft tactile-sensing upper-body robot for large object manipulation and physical human interaction. In: 2022 IEEE 5th International Conference on Soft Robotics (RoboSoft), pp. 844–851 (2022). https://doi.org/10.1109/RoboSoft54090.2022.9762117
9. Guan, Q., Stella, F., Della Santina, C., Leng, J., Hughes, J.: Trimmed helicoids: an architectured soft structure yielding soft robots with high precision, large workspace, and compliant interactions. npj Robot. **1**(1), 4 (2023). https://doi.org/10.1038/s44182-023-00004-7
10. Hilts, W.W., Szczecinski, N.S., Quinn, R.D., Hunt, A.J.: A dynamic neural network designed using analytical methods produces dynamic control properties similar to an analogous classical controller. IEEE Control Syst. Lett. **3**(2), 320–325 (2019). https://doi.org/10.1109/LCSYS.2018.2871126
11. Hofer, M., Spannagl, L., D'Andrea, R.: Iterative learning control for fast and accurate position tracking with an articulated soft robotic arm. In: 2019 IEEE/RSJ International Conference on Intelligent Robots and Systems (IROS), pp. 6602–6607. IEEE, Macau, China (2019). https://doi.org/10.1109/IROS40897.2019.8967636
12. Hunt, A., Szczecinski, N., Quinn, R.: Development and training of a neural controller for hind leg walking in a dog robot. Front. Neurorobot. **11**, (2017). https://doi.org/10.3389/fnbot.2017.00018
13. Jordan, I.D., Sokół, P.A., Park, I.M.: Gated recurrent units viewed through the lens of continuous time dynamical systems. Front. Comput. Neurosci. **15**, (2021). https://doi.org/10.3389/fncom.2021.678158

14. Kemp, C.C., Edsinger, A., Torres-Jara, E.: Challenges for robot manipulation in human environments [grand challenges of robotics]. IEEE Robot. Autom. Mag. **14**(1), 20–29 (2007). https://doi.org/10.1109/MRA.2007.339604
15. Khan, A., Martin, P.L., Hardiman, P.: Expanded production of labor-intensive crops increases agricultural employment. Calif. Agric. **58**(1), 35–39 (2004). https://doi.org/10.3733/ca.v058n01p35
16. Kim, Y.J.: Anthropomorphic low-inertia high-stiffness manipulator for high-speed safe interaction. IEEE Trans. Rob. **33**(6), 1358–1374 (2017). https://doi.org/10.1109/TRO.2017.2732354
17. Klein, M., Kandel, E.R.: Mechanism of calcium current modulation underlying presynaptic facilitation and behavioral sensitization in *Aplysia*. Proc. Natl. Acad. Sci. USA **77**(11), 6912–6916 (1980)
18. Koch, C.: Biophysics of Computation: Information Processing in Single Neurons. Oxford University Press (1998). https://doi.org/10.1093/oso/9780195104912.001.0001
19. Lechner, M., Hasani, R., Amini, A., Henzinger, T.A., Rus, D., Grosu, R.: Neural circuit policies enabling auditable autonomy. Nat. Mach. Intell. **2**(10), 642–652 (2020). https://doi.org/10.1038/s42256-020-00237-3
20. Li, Y., Sukhnandan, R., Gill, J.P., Chiel, H.J., Webster-Wood, V., Quinn, R.D.: A bioinspired synthetic nervous system controller for pick-and-place manipulation. In: 2023 IEEE International Conference on Robotics and Automation (ICRA), pp. 8047–8053 (2023). https://doi.org/10.1109/ICRA48891.2023.10161198
21. Li, Y., Webster-Wood, V.A., Gill, J.P., Sutton, G.P., Chiel, H.J., Quinn, R.D.: A synthetic nervous system controls a biomechanical model of *Aplysia* feeding. In: Biomimetic and Biohybrid Systems, pp. 354–365. Springer (2022)
22. Lu, H., McManus, J.M., Cullins, M.J., Chiel, H.J.: Preparing the periphery for a subsequent behavior: motor neuronal activity during biting generates little force but prepares a retractor muscle to generate larger forces during swallowing in *Aplysia*. J. Neurosci. **35**(12), 5051–5066 (2015). https://doi.org/10.1523/JNEUROSCI.0614-14.2015
23. Nourse, W.R.P., Jackson, C., Szczecinski, N.S., Quinn, R.D.: Sns-toolbox: an open source tool for designing synthetic nervous systems and interfacing them with cyber-physical systems. Biomimetics **8**(2), (2023). https://doi.org/10.3390/biomimetics8020247
24. Nourse, W.R.P., Szczecinski, N.S., Quinn, R.D.: A synthetic nervous system for on and off motion detection inspired by the drosophila melanogaster optic lobe. In: Biomimetic and Biohybrid Systems, pp. 364–380. Springer (2023)
25. Patan, K., Patan, M.: Neural-network-based iterative learning control of nonlinear systems. ISA Trans. **98**, 445–453 (2020). https://doi.org/10.1016/j.isatra.2019.08.044
26. Shintake, J., Cacucciolo, V., Floreano, D., Shea, H.: Soft robotic grippers. Adv. Mater. **30**(29), 1707035 (2018)
27. Sukhnandan, R., et al.: Synthetic nervous system control of a bioinspired soft grasper for pick-and-place manipulation. In: Biomimetic and Biohybrid Systems, pp. 300–321. Springer (2023)
28. Szczecinski, N.S., Getsy, A.P., Martin, J.P., Ritzmann, R.E., Quinn, R.D.: Mantisbot is a robotic model of visually guided motion in the praying mantis. Arthropod Struct. Dev. **46**(5), 736–751 (2017)
29. Szczecinski, N.S., Hunt, A.J., Quinn, R.D.: Design process and tools for dynamic neuromechanical models and robot controllers. Biol. Cybern. **111**(1), 105–127 (2017). https://doi.org/10.1007/s00422-017-0711-4

30. Szczecinski, N.S., Hunt, A.J., Quinn, R.D.: A functional subnetwork approach to designing synthetic nervous systems that control legged robot locomotion. Front. Neurorobot. **11**, 37 (2017)
31. Wang, J., Chortos, A.: Control strategies for soft robot systems. Adv. Intell. Syst. **4**(5), 2100165 (2022)
32. Webster-Wood, V.A., Gill, J.P., Thomas, P.J., Chiel, H.J.: Control for multifunctionality: bioinspired control based on feeding in *Aplysia californica*. Biol. Cybern. **114**(6), 557–588 (2020)
33. Zajac, F.: Muscle and tendon: properties, models, scaling, and application to biomechanics and motor control. Critical reviews in biomedical engineering **17**(4), 359-411 (1989), http://europepmc.org/abstract/MED/2676342
34. Zhang, B., Xie, Y., Zhou, J., Wang, K., Zhang, Z.: State-of-the-art robotic grippers, grasping and control strategies, as well as their applications in agricultural robots: a review. Comput. Electron. Agric. **177**, 105694 (2020). https://doi.org/10.1016/j.compag.2020.105694